

In Silico Spectroscopy of Tryptophan and Tyrosine Radicals Involved in the Long-Range Electron Transfer of Cytochrome c Peroxidase

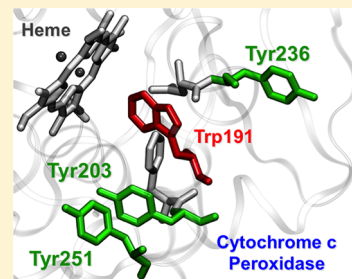
Caterina Bernini,^{†,‡} Elena Arezzini,[†] Riccardo Basosi,^{†,‡} and Adalgisa Sinicropi*,^{†,‡}

[†]Department of Biotechnology, Chemistry and Pharmacy, University of Siena, Via A. Moro 2, 53100 Siena, Italy

[‡]CSGI, Consorzio per lo Sviluppo dei Sistemi a Grande Interfase, via della Lastruccia 3, 50019, Sesto Fiorentino, Italy

S Supporting Information

ABSTRACT: Cytochrome c peroxidase (CcP) is a heme-containing enzyme that catalyzes the oxidation of the ferrocyanochrome c to ferricyanochrome c with concomitant reduction of H₂O₂ to H₂O. Its catalytic cycle involves the formation of a double oxidized species (compound I) consisting of an oxoferryl center (Fe(IV)=O) and an amino acid radical (R[•]). Here we use a quantum-mechanics/molecular-mechanics (QM/MM) computational protocol based on density functional theory (DFT) and multiconfigurational perturbation theory (CASPT2) methods to reproduce specific features of compound I EPR and UV-vis spectra. The results show that the employed QM/MM models can correctly predict the magnetic, electronic and vibrational properties of the observed amino acid radicals of compound I. Furthermore, we have been able to confirm that the principal radical species of compound I is a tryptophan cationic radical located on residue 191 (Trp191^{•+}) and that three tyrosine residues (Tyr203, Tyr236, and Tyr251), located along two possible ET pathways involving Trp191^{•+}, are possible candidates to host the secondary radical species.



INTRODUCTION

Cytochrome c peroxidase (CcP) is a heme-containing enzyme composed of 294 amino acids (32.5 kDa) involved in the mitochondria electron transport chain. It was isolated for the first time in 1940 from baker's yeast.¹ CcP catalyzes the oxidation of the ferrocyanochrome c to ferricyanochrome c with concomitant reduction of H₂O₂ to H₂O. In the first stage of the reaction (see Scheme 1), the ferric iron of the heme prosthetic group reacts with H₂O₂ to generate a hydroperoxide adduct which, in turn, gives an oxoferryl center (Fe(IV)=O) and an amino acid radical (R[•]). These double oxidized species is known as compound I (sometimes referred as compound ES).^{2,3} In the presence of electron-rich substrates, such as ferrocyanochrome c, two electron transfer (ET) reactions occur reducing both oxidized sites of compound I to the native form of CcP.

Since the 60s, several studies aimed at identifying the possible site of radical formation have been conducted.^{4–7} They have been mainly based on the use of electron paramagnetic resonance (EPR) and electronic and nuclear double resonance (ENDOR) spectroscopies. These, in fact, are the techniques of choice for the characterization of paramagnetic species. However, the complexity of the X-band (9.5 GHz) EPR spectrum of compound I, characterized by a strong g-tensor anisotropy, which is very unusual for a free organic radical, has, for a long time, prevented the secure assignment to a specific amino acid. The use of high-field (Q-band, 35 GHz) EPR and ENDOR spectroscopies allowed to assign the radical species to a tryptophan residue.^{6,8} These experiments were complemented by site-directed mutagenesis and kinetic studies showing that, among the tryptophan residues, the ones that

affect the catalytic activity of CcP and the stability of the radical of compound I are Trp191 and Trp51 (Figure 1), both in the vicinity of the heme (Fe-NTrp distances are 7.1 and 3.9 Å, respectively).^{8,9} The formation of a radical species compatible with a tryptophan residue was also revealed by UV-vis spectroscopy. Indeed, the UV-vis spectrum of CcP shows a signal in the 500–600 nm region typical of tryptophan radicals.^{10,11} Besides, the UV-vis spectra of two CcP mutants (W191F and W51F) showed a signal that could also be assigned to a tryptophan radical demonstrating, therefore, the possible formation of the radical on both tryptophan residues, Trp51 and Trp191.

The high-field EPR and ENDOR experiments also contributed to clarify that the particular shape of the X-band EPR signal of the CcP is due, in part, to a weak paramagnetic coupling of the amino acid radical with the oxoferryl heme and, in part, to the presence of a narrow signal attributed to a secondary radical species other than tryptophan. A subsequent 285 GHz EPR study¹² assigned this signal to a tyrosine radical.

To date, despite the numerous experimental research papers, the assignment of the principal radical species of compound I to Trp191 or Trp51 has not unambiguously been determined yet, not either the assignment of the tyrosine radical (the secondary radical species) to one of the 14 possible residues present in CcP.

Likewise, the chemical nature (neutral or charged) of the tryptophan radical has not unequivocally been established.

Received: March 1, 2014

Revised: July 21, 2014

Published: July 25, 2014

Scheme 1. CcP Catalytic Mechanism

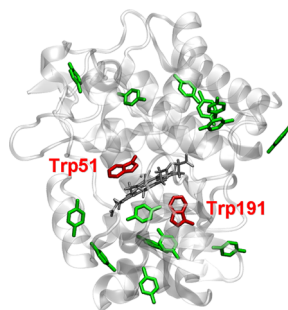
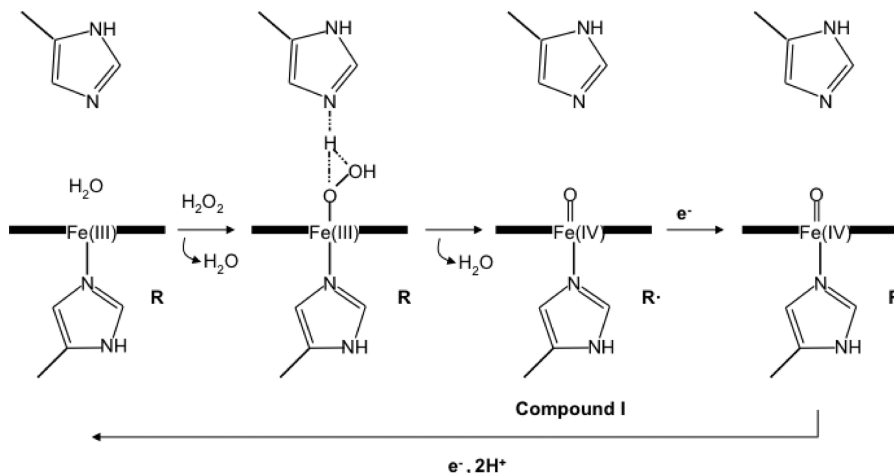


Figure 1. Heme prosthetic group (gray), Trp51 and Trp191 residues (red), and tyrosine residues (green) in CcP.

Indeed, a distinctive feature of redox-active amino acids is that they change their acidity dramatically as a function of their redox state. As a consequence, many ET reactions are coupled to proton transfer events (PCET, proton coupled electron transfer). Thus, it is evident that unveiling the nature of these radicals is crucial to clarify the details of their reactivity. This is particularly relevant for tryptophan radicals. Tyrosine radicals, in fact, are usually neutral (deprotonated) since tyrosine residues undergo, upon oxidation, a lowering of more than 12 K_a units, which is in favor of the deprotonated species.¹³

Previous theoretical studies^{14–17} on tryptophan radical models (indole, 3-methylindole, or 3-ethylindole) attempted to compute the spin density of these species and, for comparison with the experimental derived spin densities, tried to assign the observed spectral data of CcP to a protonated (cationic) or a deprotonated (neutral) radical species. Unfortunately, they were not able to give a unanimous answer, probably due to the neglect of a proper treatment of the environment and to the use of very simple models.

In this work, a quantum-mechanics/molecular-mechanics (QM/MM) strategy based on the application of density functional theory (DFT) and multiconfigurational perturbation theory (CASPT2) methods is used to reproduce specific features of EPR and UV-vis spectra of CcP compound I in order to increase our knowledge about the CcP enzyme.

The above-mentioned strategy has been previously applied to the characterization of amino acid radicals implicated in the catalytic mechanisms of other peroxidases and in the long-range ET processes of other proteins.^{18–20} The computed g-tensor, hyperfine coupling constants (hfcc's) and spin density values

allowed, in all cases, the assignment of the experimentally detected radical species to a specific protein residue and the determination of its protonation state. These studies have also made it possible to identify the environmental features that affect the magnetic, electronic, and vibrational properties of the radical species and, more particularly, to determine the specific role exerted by protein residues and solvent.

In the following, we employ the same QM/MM protocols to compute the EPR spectral parameters (g-tensors, hfcc's, and Mulliken spin densities), the absorption maxima (λ_{\max}), and the vibrationally resolved UV-vis spectra of Trp191 and Trp51 radicals, both in protonated ($\text{Trp191}^{\bullet+}$, $\text{Trp51}^{\bullet+}$) and deprotonated (Trp191^{\bullet} , Trp51^{\bullet}) forms. We show that the employed QM/MM models are capable of reproducing the main electronic, vibrational, and magnetic properties of the experimentally observed tryptophan radical. We have also been able to evaluate the spectral shifts expected for cationic and neutral tryptophan species and identify the molecular-level interactions responsible for such spectral changes. Remarkably, the obtained results allowed us to definitively confirm that the principal radical species of compound I is a tryptophan cationic radical located on residue 191 ($\text{Trp191}^{\bullet+}$). Besides, the results obtained from the computations of g-tensor values on the QM/MM models allowed us to limit the possible candidates to only three tyrosine residues (Tyr203, Tyr236, and Tyr251). Moreover, we found that these tyrosine residues are located along two possible ET pathways, which involve $\text{Trp191}^{\bullet+}$.

METHODS

Protein Setup. Initial structure for compound I of CcP (pdb code: 1ZBZ;²¹ resolution 1.29 Å) was obtained from the Protein Data Bank. Results of PROPKA3.1²² runs were used, in combination with visual inspection, to assign the protonation states of all titratable residues (aspartic acid, glutamic acid, and histidine) at the experimental pH. Missing hydrogen atoms were added by the psfgen module of VMD, version 1.9.1.²³ The protonated system, with crystallographic water molecules, was neutralized with sodium and chlorine ions (0.15 M ionic strength) and fully solvated in a rectangular box (82 × 66 × 70 Å³) of TIP3P water molecules²⁴ using the autoionize and solvate modules of VMD. Solvent boxes were created with a layer of at least 10 Å of water molecules around each protein atom (about 10000 water molecules).

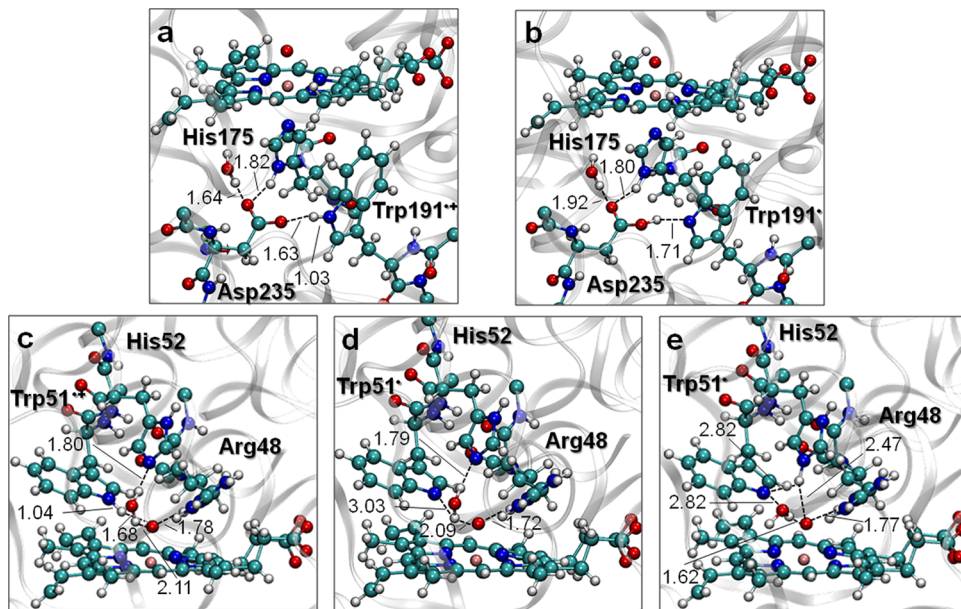


Figure 2. B3LYP/AMBER optimized geometries for Trp191^{•+} (a), Trp191[•] (b), Trp51^{•+} (c), Trp51[•] (d), and Trp51[•]–His52 (e).

Preparatory Force Field Calculations. AMBER force field^{25–27} and TIP3P water²⁴ model were used for both pure MM and hybrid QM/MM calculations. All available force field parameters and charges were taken from the parm99.dat library.²⁶ For the treatment of the heme cofactor, the published parameters for the six-coordinate heme (heme_all.db3) available from the Amber parameter database²⁸ were used. Partial atomic charges for the oxoferryl heme and the iron-coordinated His175 residue were determined at the B3LYP/6-31G* (LANL2DZ on Fe) level with Gaussian03 software package²⁹ using a restrained electrostatic potential (RESP) procedure²⁶ (Table S1 and Scheme S1). The solvated systems were relaxed by performing classical energy minimization and molecular dynamics (MD) simulations with the NAMD 2.9 code.³⁰ The positions of the hydrogen atoms and solvent water molecules were first energy minimized and equilibrated at 298 K and 1 atm for 1 ns, with a time step of 1 fs. Electrostatic interactions were taken into account using the Particle Mesh Ewald (PME) method,³¹ and periodic boundary conditions (PBC) were applied. Then, further 10 ns equilibration was carried out in which even the protein side chains were left free to equilibrate. During the MD simulations, the coordinates of the heme cofactor and protein backbone atoms were kept fixed to the crystal structure. The last snapshot at the end of the 10 ns MD equilibration run was taken and energy minimized to be used as starting structure for the following QM/MM computations.

QM/MM Calculations. All QM/MM calculations were performed with the MOLCAS 7.4 package³² coupled with a modified version of the MM package Tinker 4.2,³³ as originally described in refs 33–35. An electronic embedding (EE) scheme was applied, using hydrogen link atoms (HLA) with a scaled-charge model^{20,36–38} to treat the QM/MM boundary region (see Supporting Information for further details). Trp191 and Trp51 radicals were simulated both in the protonated (Trp191^{•+}, Trp51^{•+}) and deprotonated (Trp191[•], Trp51[•], and Trp51[•]–His52 model) forms. The QM regions employed in QM/MM calculations and the partial charges used at the frontier regions for Trp191 and Trp51 radicals are reported in

Scheme S2 and Table S2. The QM/MM models used for the simulation of tyrosine radicals have been prepared considering the results obtained from preliminary QM calculations in vacuo carried out with Gaussian09 software package³⁹ for all the 14 tyrosine residues in the protein (Figure S1), as well as by taking into account some indirect clues from the experiments.^{40–42} The QM regions and partial charges used at the frontier regions in the QM/MM models for Tyr16, Tyr23, Tyr67, Tyr203, Tyr229, Tyr236, and Tyr251 are reported in Scheme S2 and Table S3. QM/MM geometry optimizations were performed at the B3LYP/AMBER level using the 6-31G* basis set. The Morokuma's scheme, as implemented in MOLCAS 7.4,³² was applied to constrain the LA position on the line connecting the QM and the MM atoms.

EPR and UV-vis Computations. EPR magnetic parameters (\mathbf{g} -tensors, hfcc's, and Mulliken spin densities) have been computed via single-point calculations on the B3LYP/AMBER optimized structures using the ORCA2.9 program package⁴³ with an EE scheme, in which fixed MM point charges are included in the one-electron QM Hamiltonian, and the QM/MM electrostatic interactions are evaluated from the QM electrostatic potential and the MM charges. In these calculations, the B3LYP^{44–46} functional was used in combination with the Barone's EPR-II basis set.^{47–49} Indeed, the use of the B3LYP functional together with the EPR-II basis is recommended for EPR property predictions, as reported in literature.^{18,20,50–52} In order to take into account the weak exchange interaction between the radical ($S = 1/2$) and the oxoferryl heme ($S = 1$), additional calculations have been performed on the large Heme-Triad model, including the oxoferryl heme and the hydrogen-bonded His175–Asp235–Trp191 triad (Figure S2). For the Heme-Triad model, the B3LYP^{44–46} functional was used in combination with the polarized triple- ζ valence basis set TZVP.⁵³ Relativistic effects have been taken into account in the form of the zero-order regular approximation (ZORA)⁵⁴ and the spin-orbit mean-field (SOMF)⁵⁵ approximation, as reported in previous works where these approximations have been successfully applied.^{54–58} In ZORA calculations, the def2-SVP basis set was

Table 1. B3LYP/EPR-II g-Tensors (g_i) and hfcc Values (A_i , in MHz) Computed at the B3LYP/AMBER Optimized Geometries for Trp191 $^{•+}$, Trp191 $^•$, Trp51 $^{•+}$, Trp51 $^•$, and Trp51 $^•$ -His52 a

| | | g_i^a | $A_i(H_{\beta 1})^b$ | $A_i(H_{\beta 2})^b$ | $A_i(H_1)^b$ | $A_i(H_2)^b$ | $A_i(H_5)$ | $A_i(H_6)^b$ | $A_i(H_7)$ | $A_i(N_1)$ |
|-------------------|-----|---------|----------------------|----------------------|--------------|--------------|------------|--------------|------------|------------|
| Trp191 $^{•+}$ | x | 2.0033 | 18.2 | 9.6 | 1.2 | -1.7 | -6.7 | 1.1 | -4.6 | -2.0 |
| | y | 2.0024 | 19.4 | 11.0 | -14.4 | -15.4 | -18.4 | -3.4 | -15.2 | -2.4 |
| | z | 2.0023 | 26.3 | 16.2 | -19.1 | -20.2 | -24.7 | -4.3 | -22.4 | 17.1 |
| | iso | 2.0026 | 21.3 | 12.3 | -10.8 | -12.4 | -16.6 | -2.2 | -14.1 | 4.2 |
| Trp191 $^•$ | x | 2.0034 | 18.4 | 16.2 | | 3.6 | -6.12 | 1.5 | -4.2 | -1.4 |
| | y | 2.0027 | 19.5 | 16.7 | | -5.1 | -16.3 | 3.0 | -13.3 | -1.7 |
| | z | 2.0023 | 26.2 | 24.9 | | -5.8 | -21.3 | 5.6 | -19.9 | 27.7 |
| | iso | 2.0028 | 21.4 | 19.2 | | -2.4 | -14.6 | 3.4 | -12.5 | 8.2 |
| Trp51 $^{•+}$ | x | 2.0034 | 55.7 | -1.3 | 0.4 | -0.0 | -7.1 | 1.9 | -4.5 | -1.1 |
| | y | 2.0024 | 56.9 | -1.5 | -16.7 | -11.4 | -19.5 | 3.6 | -15.2 | -1.5 |
| | z | 2.0023 | 62.6 | 6.2 | -22.5 | -14.3 | -26.3 | 6.5 | -22.1 | 22.1 |
| | iso | 2.0027 | 58.4 | 1.1 | -12.9 | -8.6 | -17.6 | 4.0 | -14.0 | 6.5 |
| Trp51 $^•$ | x | 2.0044 | 67.7 | -0.02 | | 1.7 | -5.0 | 0.3 | -2.8 | -2.3 |
| | y | 2.0032 | 68.9 | 0.8 | | 5.5 | -13.4 | -0.8 | -10.3 | -2.5 |
| | z | 2.0029 | 76.4 | 9.2 | | 9.2 | -16.8 | 2.9 | -15.2 | 41.5 |
| | iso | 2.0023 | 71.0 | 3.3 | | 5.5 | -11.7 | 0.8 | -9.4 | 12.3 |
| Trp51 $^•$ -His52 | x | 2.0040 | 70.1 | 0.3 | | 0.3 | -5.3 | -0.3 | -2.9 | -0.7 |
| | y | 2.0029 | 71.5 | 1.0 | | 4.2 | -14.4 | 0.9 | -10.8 | -1.0 |
| | z | 2.0023 | 78.5 | 9.2 | | 7.7 | -18.4 | 3.5 | -15.9 | 40.3 |
| | iso | 2.0031 | 73.4 | 3.5 | | 4.1 | -12.7 | 1.4 | -9.9 | 12.9 |

^aExperimental g-tensors from ref 12 are $g_x = 2.0033$, $g_y = 2.0024$, $g_z = 2.0021$. ^bExperimental isotropic hfcc values from ref 8 are $A_i(H_{\beta 1}) = 21$, $A_i(H_{\beta 2}) = 13$, $A_i(H_1) = 16$, $A_i(H_2) = 15$, $A_i(H_6) = 5$. For tryptophan g-tensors orientation and atom numbering, see Scheme S3.

used for all the atoms except for the iron and the first coordination sphere, which includes oxygen and nitrogen atoms directly attached to the metal, and for indolic atoms for which the more accurate def2-TZVP(-f) was used.⁵⁹ The RI approximation has been applied in conjunction with a def2-SVP auxiliary basis set.⁶⁰ The integration accuracy on the metal center was increased to 14.⁵⁴ For the calculation of the EPR parameters with SOMF, a flexible basis set was used for iron (CP(PPP)⁶¹), while atoms of the first coordination shell and indole were treated with EPR-II basis set.^{47–49} The SV(P)⁶² basis set was used for the remaining atoms.

Vertical transition energies and oscillator strengths were obtained from CASPT2/ANO-S-VDZP calculations on the B3LYP/AMBER optimized geometries. The UV-vis absorption spectra were analyzed in the framework of the independent mode displaced harmonic oscillator (IMDHO) model using the “orca_asa” module⁶³ implemented in ORCA2.9⁴³ for the calculation of optical bandshapes. The spectra were simulated using a homogeneous line width of 500 cm⁻¹ and the CASPT2 vertical excitation energies. The spectra were also simulated with a reduced line width (see Supporting Information) in order to appreciate the details of the computed vibronic structures. Vibrational frequencies and gradient calculations used for UV-vis spectra simulations have been carried out with ORCA2.9⁴³ at the B3LYP/TZVP level of theory. The same strategy used to compute vertical excitation energies, oscillator strengths and UV-vis absorption spectra has already been applied in our previous work.²⁰ For more details on the simulation of the vibronic structure in optical spectra with the “orca_asa” program please refer to ref 63.

RESULTS AND DISCUSSION

Trp Radicals. QM/MM optimized models for Trp191 and Trp51 radicals in CcP are shown in Figure 2. The radicals have been simulated both in the cationic (protonated) and in the neutral (deprotonated) form. In Trp191 $^{•+}$ model (Figure 2a),

the unpaired electron is located on the positively charged 191 residue, featuring a N–H bond length of 1.03 Å and a hydrogen bond (NH···O distance of 1.63 Å) between the indolic proton and the carboxylic oxygen of the nearby Asp235 residue. The latter residue is in turn hydrogen-bonded to the iron-coordinated His175, thus forming the hydrogen-bonded triad (His175–Asp235–Trp191). In the neutral Trp191 $^•$ model (Figure 2b), the indolic proton has been transferred to Asp235 residue, which is still tightly hydrogen bonded to the Trp191 radical with a N···H distance of 1.71 Å. In the Trp51 $^{•+}$ model (Figure 2c), the positively charged radical on residue 51 is hydrogen-bonded to the ferryl oxygen with a NH···O distance of 1.68 Å and featuring a N–H bond length of 1.04 Å. In the case of the neutral species (Trp51 $^•$ model; Figure 2d), the indolic proton has been removed, thus assuming the proton release into water solution following tryptophan radical deprotonation or it has been transferred to the nearby His52 (Trp51 $^•$ -His52 model; Figure 2e). In both cases the deprotonated Trp51 radical is involved in weak hydrogen bonds with solvent water molecules or with the newly protonated His52 (in Trp51 $^•$ -His52 model).

EPR. Tryptophan radicals are characterized by a small g-tensor anisotropy, which is a common feature of organic π -radicals with spin densities only on carbon or nitrogen atoms.⁶⁴ Typical g-tensor values of tryptophan radicals are $g_x \sim 2.0033$ –2.0036, $g_y \sim 2.0024$ –2.0027, and $g_z \sim 2.0022$ (Scheme S3 for tryptophan g-tensors orientation and numbering scheme). As already pointed out in prior computational works,^{18,20,65–67} the g-factor anisotropy is increased when tryptophan radical cation is deprotonated to a neutral species. In particular, the g_x component of the radical is decreased when the length of the N–H bond becomes shorter, that is, the bond becomes stronger. From the experimental point of view, the small g-tensor anisotropy of tryptophan radicals can be fully resolved only by using ultrahigh field and frequency EPR spectroscopy. This goal has been achieved only recently by Stoll et al.,⁶⁸

which obtained a complete separation of the three principal g-tensor components of tryptophan neutral radicals in *Pseudomonas aeruginosa* Azurin using an EPR instrument at 700 GHz and 25 T. Such highly resolved experimental g-tensor values have been correctly reproduced (within 130 ppm) in a recent paper²⁰ where the same protocol used in this work has been applied.

The B3LYP/EPR-II computed g-tensors at the B3LYP/AMBER optimized geometries for Trp191^{•+}, Trp191[•], Trp51^{•+}, Trp51[•], and Trp51[•]-His52 are gathered in Table 1. As expected, the computed g-tensor anisotropy for the cationic species is smaller than the one computed for the neutral radicals. Moreover, the g-tensors for Trp191^{•+} and Trp51^{•+} are in good agreement with the experimental values ($g_x = 2.0033$, $g_y = 2.0024$, $g_z = 2.0021$) reported in ref 12. The agreement between computed and experimental data for the corresponding deprotonated radicals is instead less satisfactory. This finding supports the assignment of the EPR signal to a cationic species (Trp191^{•+} or Trp51^{•+}).

The higher g-tensor anisotropy for the neutral tryptophan radicals compared to the cationic species is accompanied by an increase in Mulliken spin density on C₃ and N₁ and by a concomitant decrease of the spin density on C₂. In Table S4, B3LYP/EPR-II computed Mulliken spin densities are compared with McConnell-derived π -spin densities from experimental isotropic hfcc values.⁸ Also, in this case, the fit with the experimental data is improved for the charged species.

In order to discriminate between Trp191^{•+} and Trp51^{•+} and assign unequivocally the EPR spectrum to only one of the two species, it is necessary to inspect the β -methylene protons' hfcc values. Indeed, it is well-known that the EPR spectra of tryptophan radicals are dominated by the $A(H_{\beta 1})$ and $A(H_{\beta 2})$ values, which are dependent on the overlap with the spin density on C₃ and, hence, on the indole ring rotation angle ϕ , defined by the C_α-C_β-C₃-C₂ dihedral angle. As a consequence, for $\phi \sim 90^\circ$, the two β -methylene protons share the same amount of C₃ spin density and the hfcc values are expected to be the same. The greater is the deviation in the value of ϕ from 90°, the larger is the difference between $A(H_{\beta 1})$ and $A(H_{\beta 2})$ values.

In our case, B3LYP/EPR-II computed values for $A(H_{\beta 1})$ and $A(H_{\beta 2})$ are much closer to each other for Trp191^{•+} than for Trp51^{•+} (Table 1). This is in accord with the different orientation of the two radicals in the protein ($|\phi| \sim 90^\circ$ for Trp191^{•+} and $|\phi| \sim 120^\circ$ for Trp51^{•+}). In particular, the computed $A_{iso}(H_{\beta 1})$ and $A_{iso}(H_{\beta 2})$ values for Trp191^{•+} (21.3 and 12.3 MHz) are consistent with a structure having ϕ close to 90° and show a better fit to the experimental values (21 and 13 MHz)⁸ compared to the same values computed for Trp51^{•+} (58.4 and 1.1 MHz). Indeed, these latter values agree with a geometry featuring one of the two β -methylene protons much closer to the indole plane. Thus, computed EPR parameters for the radical species of Trp191 and Trp51, in comparison with available experimental results, strongly suggest that the primary amino acidic radical species in CcP is ascribable to Trp191 residue.

Another goal of this work was to take into account in the calculations the weak exchange interaction between the tryptophan radical ($S = 1/2$) and the oxoferryl heme ($S = 1$) that is responsible for the anomalous EPR absorption envelope of CcP showing a maximum at $g = 2.01$ and a shoulder to lower field at $g = 2.04$. To this end, additional calculations have been performed on a large model (Heme-Triad in Figure S2),

including the oxoferryl heme and the hydrogen-bonded His175-Asp235-Trp191 triad. Results obtained for the Heme-Triad model, both nonrelativistic ($g_x = 2.0439$, $g_y = 2.0211$, $g_z = 2.0184$) and with the inclusion of relativistic effects, using the zero-order regular approximation (ZORA;⁵⁴ $g_x = 2.0408$, $g_y = 2.0209$, $g_z = 2.0199$) or the spin-orbit mean-field (SOMF)⁵⁵ approximation ($g_x = 2.0404$, $g_y = 2.0221$, $g_z = 2.0204$) are in nice agreement with the g-tensor values (2.04, 2.01, 2.01) used by Hoffman^{8,9} to simulate the EPR spectrum of CcP. This finding further proves the reliability of the QM/MM models and strategy used, even more in taking into account the interactions between paramagnetic centers.

UV-vis. Complementary and useful information for the characterization of tryptophan radicals and the discrimination of the protonation state can also be provided by UV-vis spectroscopy. Indeed, UV-vis absorption spectra of tryptophan radicals in aqueous solution obtained by pulse radiolysis studies show a peak at 560 nm for the cation species and at 510 nm for the neutral species.⁶⁹ Similarly, the UV-vis absorption spectra obtained from the photofragmentation of peptides containing tryptophan radicals in the gas phase exhibit a single band at 590 nm for the cation species, significantly red-shifted compared to the band at 473 nm recorded for the neutral species.^{70,71} Differently, in the protein environment of two *Pseudomonas aeruginosa* Azurin mutants (Az48W and ReAz108W), the UV-vis absorption spectrum of a neutral tryptophan radical features a double-band pattern with two relatively narrow peaks at 486 and 516 nm for Az48W and at 510 and 537 nm for ReAz108W.⁷²

Like in Azurin proteins, the UV-vis absorption spectrum of compound I in CcP is characterized by two peaks at 530 and 560 nm.^{10,11,73} Here, using the same computational approach adopted for Azurin,²⁰ absorption maxima λ_{max} (nm), excitation energies E_{exc} (eV), and oscillator strengths (f_{osc}) have been determined at the *state-of-the-art* CASPT2 level of theory (with a CAS(9,9) and a CAS(11,10) expansion in the reference CASSCF wave function) on the B3LYP/AMBER equilibrium geometries of Trp191 and Trp51 radicals using the ANO-S-VDZP basis set (CASSCF and MS-CASPT2 data are reported in Table S5). Computational results reported in Table 2 clearly demonstrate that, similarly to Azurin, the visible absorption spectrum of CcP originates from a single $D_0 \rightarrow D_2$ electronic transition. Indeed, the only other electronic transition with non-negligible oscillator strength is the $D_0 \rightarrow D_4$, with an absorption maximum around 300 nm, consistent with the presence of a peak in that region of the experimental spectrum. The other $D_0 \rightarrow D_3$ and $D_0 \rightarrow D_1$ transitions are both very weak, the latter corresponding to an absorption in the IR region. Besides, the simulation of the vibrationally resolved electronic spectra in the 400–700 nm range (see Figure 3 and the Methods section for details on the protocol used to simulate the spectra) shows that the observed double band line shape of the visible absorption spectrum of CcP is correctly reproduced when taking into account its vibrational progression. Normal modes with the largest FC factors are reported in Tables S6–S9 and represented in Figures S4, S6, S8, and S10.

The CASPT2/ANO-S-VDZP//B3LYP/6-31G* computed vertical excitation energies fall under the experimental peak at lower wavelengths and thus the computed values are compared with the observed value for this peak (530 nm, 2.34 eV). However, a straightforward evaluation of the accuracy in reproducing the experimental data may be provided by

Table 2. CASPT2/ANO-S-VDZP//B3LYP/6-31G*
Absorption Maxima λ_{max} (nm), Excitation Energies E_{exc} (eV),
and Oscillator Strengths (f_{osc}) for Trp191^{•+}, Trp191[•],
Trp51^{•+}, Trp51[•], and Trp51[•]-His52 Models

| | | λ_{max} | E_{exc} | f_{osc} |
|---------------------------|---------------------------------|------------------------|------------------|------------------|
| Trp191 ^{•+} | D ₀ → D ₁ | 1119 | 1.11 | 0.0001 |
| | D ₀ → D ₂ | 544 | 2.28 | 0.0368 |
| | D ₀ → D ₃ | 340 | 3.66 | 0.0086 |
| | D ₀ → D ₄ | 313 | 3.92 | 0.0809 |
| Trp191 [•] | D ₀ → D ₁ | 1034 | 1.20 | 0.0000 |
| | D ₀ → D ₂ | 493 | 2.52 | 0.0182 |
| | D ₀ → D ₃ | 333 | 3.73 | 0.0073 |
| | D ₀ → D ₄ | 299 | 4.16 | 0.0227 |
| Trp51 ^{•+} | D ₀ → D ₁ | 1225 | 1.01 | 0.0001 |
| | D ₀ → D ₂ | 562 | 2.21 | 0.0418 |
| | D ₀ → D ₃ | 350 | 3.55 | 0.0083 |
| | D ₀ → D ₄ | 307 | 4.04 | 0.0713 |
| Trp51 [•] | D ₀ → D ₁ | 1112 | 1.12 | 0.0001 |
| | D ₀ → D ₂ | 475 | 2.61 | 0.0151 |
| | D ₀ → D ₃ | 338 | 3.67 | 0.0069 |
| | D ₀ → D ₄ | 303 | 4.10 | 0.0067 |
| Trp51 [•] -His52 | D ₀ → D ₁ | 1134 | 1.09 | 0.0000 |
| | D ₀ → D ₂ | 490 | 2.53 | 0.0175 |
| | D ₀ → D ₃ | 342 | 3.64 | 0.0070 |
| | D ₀ → D ₄ | 301 | 4.13 | 0.0117 |

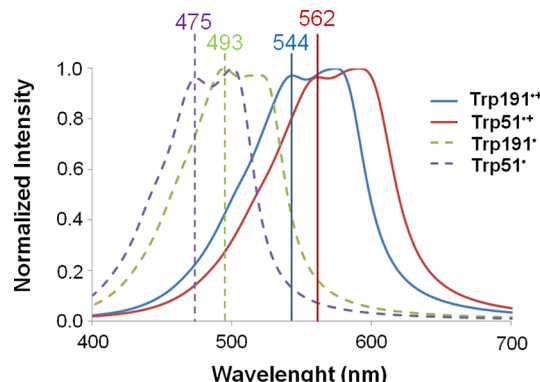


Figure 3. Simulation of UV-vis spectra for the D₀ → D₂ electronic transition in Trp191^{•+}, Trp191[•], Trp51^{•+}, and Trp51[•] models using a homogeneous broadening $\Gamma = 500 \text{ cm}^{-1}$. See also the simulated spectra with a reduced line width in Figures S3, S5, S7, and S9.

comparing computed excitation energies for Trp191 and Trp51 radicals with the measured absorption maxima for W51F (525 nm) and W191F (537 nm) mutants of CcP,^{10,11} respectively. Indeed, in the mutants, the selective substitution of Trp51 (in W51F) and Trp191 (in W191F) with a Phe residue allowed the suppression of the respective contribution to the UV-vis spectrum.

It is evident that the charged species reproduce the observed values better than the neutral species. Indeed, the computed excitation energies for the charged species are shifted to lower energies of only 0.08–0.10 eV with respect to the experimental ones. On the other hand, the excitation energies for the neutral species are shifted to higher values by 0.16–0.30 eV (these energy differences are schematically summarized in Figure S11). The computed trend, with red-shifted maxima for charged radicals, is perfectly in accord with the difference observed experimentally for cationic and neutral tryptophan radicals in other systems.^{69–71} Besides, the accuracy ($\leq 0.1 \text{ eV}$)

in reproducing the observed absorption maxima obtained for the cationic species is a further evidence of the charged nature of the tryptophan radical in CcP compound I. The obtained results also underline the sensitivity of the methodology used with respect to environmental changes. Indeed, the bathochromic shift of 12 nm (0.05 eV) going from W51F (525 nm, 2.36 eV) to W191F (537 nm, 2.31 eV) is well reproduced by the computed red-shift of 18 nm (0.07 eV) going from Trp191^{•+} (544 nm, 2.28 eV) to Trp51^{•+} (562 nm, 2.21 eV). Environmental effects are also evident for the neutral species for which a red-shift of 15 nm (0.08 eV) is computed when Trp51[•] experiences the positive charge of the protonated His52 in the Trp51[•]-His52 model. An analogous red-shift of 18 nm (0.10 eV) is predicted going from Trp51[•] to Trp191[•].

In order to investigate the causes of these environmental effects, it is useful to inspect the CASSCF/ANO-S-VDZP Mulliken spin population values that mainly contribute to the total spin population for D₀ and the excited D₂ states responsible for the observed electronic transition (D₀ → D₂; Figure 4, top). For the neutral species, Trp191[•] and Trp51[•], the transition is characterized by a displacement of the spin population toward the benzene ring that is holding the radical center in the D₂ excited state. This displacement is accompanied by a change in the charge distribution (see Figure 4, bottom). In particular, the D₂ excited state features a more negative pyrrole moiety and a more positive benzene ring with respect to D₀. Thus, upon excitation, tryptophan neutral radical undergoes an increased charge separation that can be stabilized by a suitable polar environment. This effect may justify the diverse responses of Trp191[•] and Trp51[•] to their different environments. Indeed, the D₂ excited state of Trp191[•], tightly hydrogen bonded to the nearby Asp235, should be stabilized more than the D₂ of Trp51[•], not involved in such hydrogen bonding interactions. This results in a decreased D₀–D₂ energy gap for Trp191[•] and a corresponding red-shift of the UV-vis absorption maximum. The same argument can be used to explain the red-shift caused by the presence of a positive charge (the positively charged His52) in the vicinity of the negatively charged pyrrole ring of Trp51[•] in the Trp51[•]-His52 model.

For the charged species as well, Trp191^{•+} and Trp51^{•+}, the transition is characterized by a displacement of the spin population toward the benzene ring with a change in the charge distribution (Figure 4). Here, the D₂ excited state features a less positive pyrrole moiety and a more positive benzene ring with respect to D₀. The decrease of the positive charge on the pyrrole ring may justify the lower stability of the D₂ excited state of Trp191^{•+}, due to the presence of the nearby negatively charged side chain of Asp235. Indeed, for Trp191^{•+}, we found an increased D₀–D₂ energy gap coherently with a blue-shift of the UV-vis absorption maximum.

Tyr Radicals. Tyrosine radicals show a significantly larger g-tensor anisotropy than tryptophan radicals due to the large spin density on oxygen.⁶⁴ In fact, the considerable spin-orbit coupling constant of oxygen, compared to nuclei such as nitrogen or carbon ($\xi = 151, 76$, and 28 cm^{-1} for O, N, and C, respectively), gives rise to a bigger Δg_x ($\Delta g_x = g_x - g_{\text{electron}}$).^{64,74,75} It is well-known, both from experimental^{74,76,77} and theoretical studies,^{18,51,66,67,78} that the hydrogen-bonding status and protein electrostatic environment of tyrosine radicals can be assessed from their g-tensor values. In particular, the g_x component (C₄–O direction, see Scheme S4) is sensitive to even relatively weak electrostatic perturbations and especially to

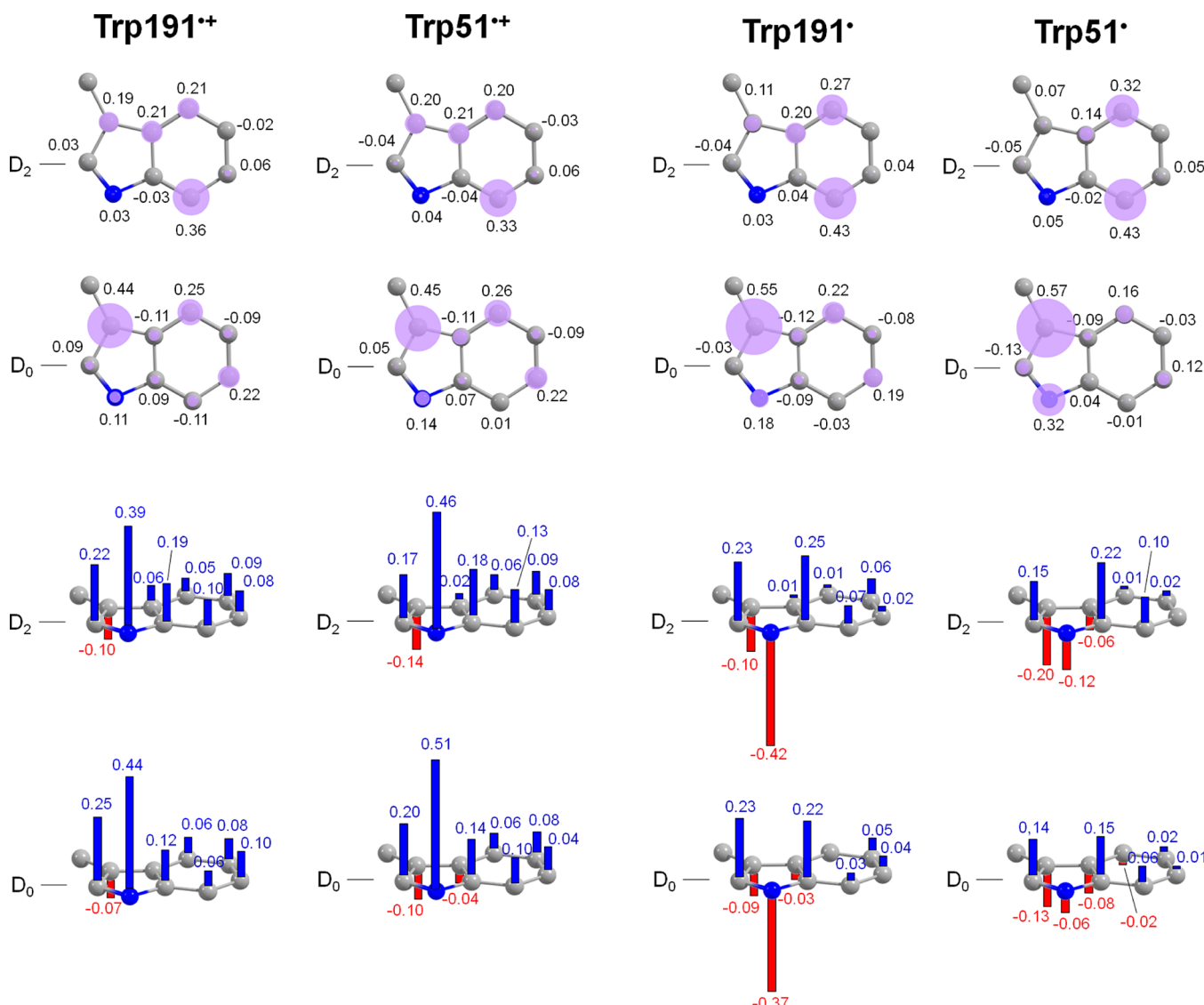


Figure 4. Mulliken spin population values (top) and charge distribution (bottom) of the D_0 and D_2 states for tryptophan cation radicals ($\text{Trp}191^{\bullet+}$ and $\text{Trp}51^{\bullet+}$, left) and for tryptophan neutral radicals ($\text{Trp}191^{\bullet}$ and $\text{Trp}51^{\bullet}$, right) computed at their B3LYP/AMBER equilibrium geometries. A fraction of positive (blue) and negative (red) charges is shown with colored bars along with the corresponding values (atomic charges with hydrogens summed into heavy atoms). The total Mulliken spin population is equal to 1, and the total Mulliken charge is equal to 0, adding the small contributions from the remaining QM atoms.

hydrogen bonds between the carbonyl group of tyrosine and the protein environment. In the literature, the g_x values for tyrosine radicals range from 2.0065, due to a strong hydrogen bond, to 2.0094, in a nonpolar and non-hydrogen-bonding environment.¹³ The g_z component (ring perpendicular direction) is approximately constant for all tyrosine radicals, with a value of \sim 2.00212, while the g_y component (mutually perpendicular to the other two components) is relatively insensitive to environmental effects and has an approximate value of 2.0045.^{13,78}

By using high-field EPR spectroscopy, it is possible to resolve g -anisotropies of tyrosine radicals and measure g -values with high accuracy. Furthermore, using computational approaches, the observed differences in g -tensor values can be correlated to the variation in hydrogen-bonding network surrounding the radical. Thus, a precise measure of the g -values for tyrosine radicals, combined with computational methods, can be used to obtain detailed information regarding the chemical environ-

ment of the radical species. Such a combined computational–experimental approach has already been used successfully in several works,^{18,51,52,66,78–81} and it has been applied here to investigate the transient tyrosine radical that is formed 60 s after the addition of 1 equiv of hydrogen peroxide to CcP and disappeared after 1 h.

Highly resolved experimental EPR data for CcP Compound I and for a CcP mutant (W191G) in which Trp191 was replaced by a glycine residue have been obtained by Ivancich et al.¹² Interestingly, the g -values of the radical ($g_x = 2.00644$, $g_y = 2.00436$, and $g_z = 2.00208$) used to simulate the difference spectrum (i.e., the spectrum that was obtained by subtracting the high-field spectra of CcP compound I measured after 60 and 15 s mixing time) in the native enzyme, as well as those determined for the W191G mutants ($g_x = 2.00660$, $g_y = 2.00425$, and $g_z = 2.00208$), are essentially identical to those obtained for a tyrosine radical generated by γ -irradiation of Tyr-HCl crystals ($g_x = 2.00658$, $g_y = 2.00404$, and $g_z = 2.00208$),

whose very low g_x value can be directly correlated to an electropositive electrostatic effect of the environment on the tyrosine radical. Besides, the broadening of the g_x portion of the high-field spectrum (with a Gaussian width of 0.0005) points out that the electrostatic environment should be distributed, similar to that of tyrosine radicals in Photosystem II ($\text{Tyr}^{\bullet}\text{z}$)^{13,82} and bovine liver catalase.⁷⁸ Based on this experimental evidence, several tyrosine candidates have been proposed in the past. Residues at positions 251, 244, 187, and 153 have been selected among those sites who meet the criteria of (i) a positive electrostatic environment due to the effect of hydrogen bond donors and/or positive charges in the surroundings and (ii) nearness on the proximal side to the heme iron (<17 Å).¹² Site-directed mutagenesis in conjunction with electrospray mass spectrometry, however, provided evidence in favor of Tyr236 as the most likely radical site.^{41,42} Nevertheless, other studies based on electrospray mass spectrometry indicated Tyr39 and Tyr153 as two additional residues capable of forming radical centers upon reaction of CcP with hydrogen peroxide.⁴⁰ Thus, far, there is only limited and inconclusive information regarding the tyrosine residue responsible for the narrow signal in the EPR spectrum of CcP compound I.

Here, as a first step to identify the tyrosine residue, which gives origin to the secondary radical species in CcP, QM models for all the 14 tyrosine residues in CcP have been constructed. In vacuo calculations have been initially performed on these QM models that have been extracted from the MD equilibrated structure of CcP (Figure S1). Each model has been defined such as to include the tyrosine of interest along with its most likely proton acceptor. In the case of solvent-exposed tyrosine residues, the water molecules closest to the phenoxy oxygen (within 4 Å) have also been included in the calculation. Geometry optimizations have been carried out at the B3LYP/6-31G* level, constraining the ring rotation angle ϕ (i.e., the $C_{\alpha}-C_{\beta}-C_1-C_2$ dihedral angle) to the value of the equilibrated protein structure. EPR magnetic parameters have been computed on the optimized geometries using the B3LYP functional and the EPR-II basis set (see Table S10 for the complete set of computed g -values and hfcc's).

In Figure 5, computed g_x values (see blue rhombs) for the 14 tyrosine radical models are gathered and compared with the highly resolved experimental g_x component (shown as dashed line). From the comparison it is evident that a good match is

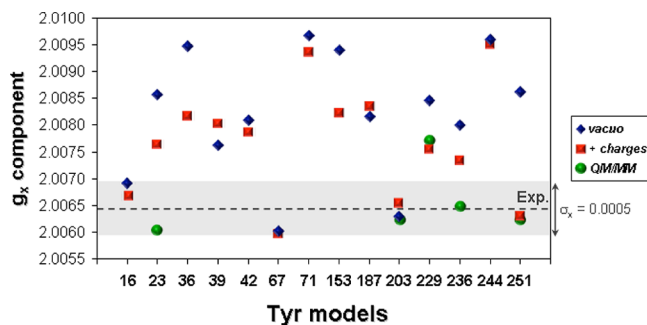


Figure 5. Comparison between experimental and B3LYP/EPR-II computed g_x values for the 14 QM models of CcP tyrosine radicals obtained in vacuo (blue rhombs), in the presence of the electrostatic effect of heme and protein residues within 10 Å of tyrosine radical (red squares) and for the QM/MM models of Tyr23*, Tyr203*, Tyr229*, Tyr236*, and Tyr251* (green circles).

found only in three cases: Tyr16* ($g_x = 2.00690$), Tyr67* ($g_x = 2.00602$), and Tyr203* ($g_x = 2.00629$). The extremely low g_x value obtained for these models arises from a very strong hydrogen bond interaction between the phenoxy oxygen and the phenoxy proton transferred to the carbonyl group of Ile285, Val7, and Val169, respectively, with hydrogen bond distances of 1.61, 1.45, and 1.50 Å. The role of such tight hydrogen bonds in lowering the g_x value is perfectly in accord with previous works on tyrosine radicals.^{18,51,66} The proton transfer to the backbone of Ile285, Val7, and Val169 could be considered plausible taking into account the transient nature of the tyrosine radical. In fact, it gives rise to an unstable cationic complex that facilitates the PCET leading back to the reduced tyrosine residue.

The computed g_x component for all the other models is significantly higher ($g_x > 2.0075$) than the experimental value, also considering the observed Gaussian width (σ_x) of 0.0005. This is consistent with the absence of very tight hydrogen bonds in these QM models.

However, bearing in mind the potential role of the protein environment in affecting the g_x value of tyrosine radicals, the calculation of the EPR magnetic parameters for the above 14 models has been repeated by taking into account the electrostatic effect of the protein charges within 10 Å of tyrosine radical (see red squares in Figure 5). The inclusion of the protein charges causes an appreciable shift in the computed g_x component for most of the models, with the exception of Tyr16*, Tyr42*, Tyr67*, Tyr187*, Tyr203*, and Tyr244*, whose g_x values remain substantially unchanged. In particular, the insensitivity of the g_x component to the protein environment for Tyr16*, Tyr67*, and Tyr203* is a further proof that the low g_x values computed for these three models can be attributed solely to the presence of a very tight hydrogen bond interaction. As regards the other cases, the most dramatic change is registered for Tyr251*, whose g_x value moves from 2.00861 (computed in vacuo and resulting from the hydrogen bond (1.76 Å) with the Asp261 residue) to 2.00630. This effect could be ascribed to the presence of two positively charged residue in the surroundings of Tyr251* (Lys257 and Arg166), as already hypothesized, but never investigated in details, by Ivancich et al.¹² Our further analysis (see discussion below) confirms the role of these two charged residues in affecting the g_x values of Tyr251*. Nevertheless, the possible role of other charged residues nearby Tyr153*, Tyr187*, and Tyr244*, suggested by the same authors, is not confirmed by this work. In fact, computed g_x values for Tyr153*, Tyr187*, and Tyr244* are all larger than 2.0080, and in the case of Tyr187* and Tyr244*, they do not differ considerably from the value computed in vacuo. Thus, the QM calculations made on the 14 tyrosine models, both in vacuo and in the presence of the protein charges, allowed to select Tyr16*, Tyr67*, Tyr203*, and Tyr251* as most probable candidates for the transient tyrosine radical in CcP. In addition to the above-mentioned residues, Tyr23*, Tyr229*, and Tyr236* have been taken into account because of their g_x values, which are close to the upper limit of the Gaussian width (~0.0070). Moreover, as stated above, in favor of Tyr236, there is also experimental evidence.^{41,42}

The seven selected tyrosine candidates have been the subjects of further QM/MM computations whose results are given below in Figures 6 and 7 and in Table S11.

For Tyr16* and Tyr67*, the QM/MM geometry optimizations show that the phenoxy proton, initially placed on the carbonyl group of Ile285 and Val7 residues, respectively, and

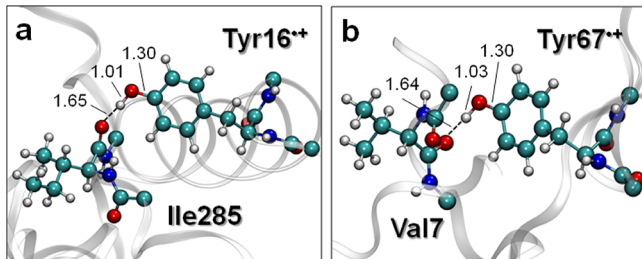


Figure 6. B3LYP/AMBER optimized geometries for tyrosine radicals: 16 (a) and 67 (b).

hydrogen bonded to the phenoxyl oxygen, is transferred back to the tyrosine residue, leading to unlikely tyrosine cation radicals (Figure 6a,b). Thus, $\text{Tyr}16^{\bullet}$ and $\text{Tyr}67^{\bullet}$ can be ruled out by the QM/MM investigation.

On the contrary, the QM/MM geometry optimization for $\text{Tyr}203^{\bullet}$ provides the stabilization of the proton located on the carbonyl group of Val169 with a very short $\text{Tyr}203\text{O}^{\bullet}\cdots\text{H}$ hydrogen bond distance of 1.40 Å (Figure 7b). The computed g_x component ($g_x = 2.00622$) for $\text{Tyr}203^{\bullet}$ (see green circles in Figure 5) does not differ from the value computed for the QM model, confirming the hydrogen bond interaction as the main contribution to the g_x value of $\text{Tyr}203^{\bullet}$.

The QM/MM optimized geometries for $\text{Tyr}23^{\bullet}$ and $\text{Tyr}251^{\bullet}$ (Figure 7a,e), compared to the QM models optimized in vacuo, show shorter hydrogen bond lengths with $\text{Tyr}23\text{O}^{\bullet}\cdots\text{HO}(\text{Glu}118)$ and $\text{Tyr}251\text{O}^{\bullet}\cdots\text{HO}(\text{Asp}261)$ distances of 1.64 and 1.46 Å, respectively. Besides, while the g_x value ($g_x = 2.00623$) computed for the QM/MM model of $\text{Tyr}251^{\bullet}$ is in accord with the value (2.00630) computed for the “QM + charges” model, the g_x value of $\text{Tyr}23^{\bullet}$ undergoes a substantial reduction in the protein environment ($g_x = 2.00603$), which was not possible to obtain from the QM model, even with the inclusion of the protein charges. Likewise, the g_x value ($g_x = 2.00646$) computed for the QM/MM model of $\text{Tyr}236^{\bullet}$ (Figure 7d) is significantly lower than that computed for the “QM + charges” model (2.00733) and it is now in perfect agreement with the

experiment. The lower g_x values computed for the QM/MM models of $\text{Tyr}23^{\bullet}$ and $\text{Tyr}236^{\bullet}$, compared to g_x values computed for the “QM + charges” models, could be ascribed to the electrostatic effect due to the whole protein environment and, in part, to the different scheme (QM/MM vs QM + charges) used.

Differently from $\text{Tyr}236^{\bullet}$, the solvent exposed $\text{Tyr}229^{\bullet}$ (Figure 7c) features a g_x value ($g_x = 2.00766$) substantially unchanged compared to that computed for the “QM + charges” model. This value is significantly higher than the experimental evidence (Figure 5), and thus, this residue can be excluded from the candidates’ list.

It is interesting to establish if the observed shifts in the g_x values for these radicals in the protein environment are due to a change in the radical geometry, to electrostatic effects caused by the protein/solvent environment, or to specific molecular interactions such as hydrogen bonding with residues or solvent molecules. To this end, the g_x values have been computed for the isolated radicals, taken with their protein-optimized geometries, and for several subsystems obtained by adding to the isolated radicals the effects of the protein residues or solvent molecules (each fragment is taken with the geometry optimized for the full protein). The complete results of the detailed analysis of the factors determining the computed g_x values for the QM/MM models of $\text{Tyr}23^{\bullet}$, $\text{Tyr}236^{\bullet}$, and $\text{Tyr}251^{\bullet}$ are presented in Table S12. For all the tyrosine radicals, the presence of a hydrogen bond donor is necessary to bring the g_x value below 2.01. For $\text{Tyr}23^{\bullet}$, the g_x value of 2.00798 computed for the $\text{Tyr}23 + \text{Glu}118$ model, compared to that (2.00856) computed for the QM model in vacuo is in accord with the reduction of the $\text{Tyr}23\text{O}^{\bullet}\cdots\text{HO}(\text{Glu}118)$ hydrogen bond distance from 1.79 to 1.64 Å in the protein environment. However, this value is still too high compared to the experimental data and cannot be the sole cause of the drop of the g_x value computed for $\text{Tyr}23^{\bullet}$ inside the full protein (2.00603). Only the inclusion of additional hydrogen bond interactions with nearby protein residues ($\text{Gln}117$, $\text{Thr}288$, $\text{Gln}20$, and $\text{Gln}292$; see Figure 7a), and the electrostatic effect

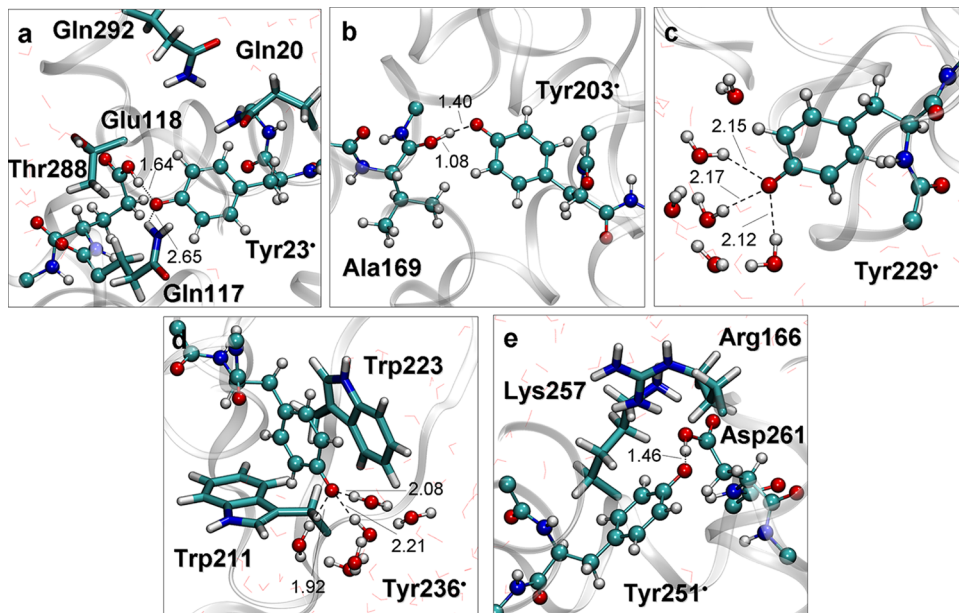


Figure 7. B3LYP/AMBER optimized geometries for tyrosine radicals: 23 (a), 203 (b), 229 (c), 236 (d), and 251 (e).

of the nearest water molecules, allows approaching the value obtained for the full QM/MM model. Likewise, for Tyr251[•], the decrease in the g_x value from 2.00861 (QM model in vacuo) to 2.00774 (Tyr251 + Asp261) can be explained by the reduction of the Tyr251O[•]···HO(Asp261) distance from 1.76 to 1.46 Å. However, it is only by taking into account the electrostatic effect of the positively charged Lys257 and Arg166 (see Figure 7e), as anticipated before, that it is possible to reach a g_x value ($g_x = 2.00637$) close to that computed for Tyr251[•] inside the full protein (2.00623). In the case of Tyr236[•], the hydrogen-bonded QM water molecules (Tyr236 + wat_{QM}) do not cause a significant shift in the g_x value ($g_x = 2.00811$) compared to that observed for the QM model in vacuo ($g_x = 2.00799$). It is mainly the effect of two nearby tryptophan residues (Trp211 and Trp223, see Figure 7d; $g_x = 2.00767$) and of the heme that causes a considerable reduction of the g_x value ($g_x = 2.00689$). In conclusion, QM/MM computed g_x values suggest that only Tyr23[•], Tyr203[•], Tyr236[•], and Tyr251[•] could be responsible for the secondary radical species in CcP.

Unfortunately, the computed hfcc values (shown in Table S11) cannot be used, as we did before for the tryptophan radicals, to discriminate among the tyrosine residues since the available experimental hfcc values are those of the W191G mutant of CcP.¹² Thus, a comparison with our computed values for the native enzyme is not straightforward and, in our opinion, could not be strictly used to this scope. This is due to the fact that the $A(H_{\beta 1})$ and $A(H_{\beta 2})$ values, which dominate the EPR spectra of tyrosine radicals, could be affected by even small differences in the phenoxy ring orientation between the mutant and native enzyme. Anyway, from the inspection of the $A(H_{\beta 1})$ and $A(H_{\beta 2})$ values, it seems that a reasonable agreement with the experimental values is found only in the case of Tyr236[•]. This, in principle, could exclude all the other candidates from the list of possible secondary transient species of Compound I.

As final consideration, it is worth to say that, among the four remaining candidates (Tyr23[•], Tyr203[•], Tyr236[•], and Tyr251[•]), Tyr23[•] is probably the less likely radical site because of its distance from the heme (>21 Å) and from the principal radical species, Trp191^{•+} (~24 Å). On the other hand, Tyr203[•], Tyr236[•], and Tyr251[•] are closer to the heme (<19 Å) and in a peculiar position with respect to Trp191 (Figure 8). In particular, Tyr236 is connected by a peptide bond to Asp235 residue, which is directly involved in a hydrogen bond interaction with Trp191. As a result, an electron transfer could be envisioned via a σ -bond tunneling through the “Trp191–Asp235–Tyr236” pathway. On the other hand, the π -system of Tyr203 can interact with that of Phe202 (Figure 8)

which, in turn, is in contact with the π -system of Trp191. This kind of T-shaped π stacking interaction could favor the electron migration along the other possible Trp191–Phe202–Tyr203 pathway. Furthermore, the close proximity of Tyr203 to Tyr251 could explain the extra possible delocalization of the unpaired electron on this latter residue.

CONCLUSIONS

In this work, the in silico characterization of the amino acid radical species involved in the long-range ET processes of CcP has been carried out for the first time. In particular, B3LYP/AMBER models have been used to successfully reproduce the magnetic properties of the observed amino acid radicals of compound I along with the electronic and vibrational properties of the potentially involved Trp amino acid radicals.

The obtained results allowed us to confirm that the principal transient species consists of a cationic Trp radical located on residue 191 (Trp191^{•+}), giving answer to a scientific discussion that lasted more than 20 years. Furthermore, in a model that includes the oxoferryl heme and the His175–Asp235–Trp191 triad, the computed g-tensor values, in both the relativistic and the nonrelativistic treatment, are in good agreement with the experimental values and are coherent with a weak exchange interaction between the Trp radical ($S = 1/2$) and the oxoferryl heme ($S = 1$).

The DFT/AMBER strategy has been also applied to simulate tyrosine radicals within the protein matrix of CcP. The computed g_x values permitted to suggest that, among the 14 tyrosine residues present in the CcP, only three tyrosine residues (Tyr203, Tyr236, and Tyr251) are the possible candidate to host the secondary radical species that contributes to about 10% of the EPR spectrum of the CcP. Additionally, we found that these tyrosine residues are located in a advantaged position with respect to ET processes. In fact, they reside along two possible ET pathways, which involves Trp191^{•+}. More specifically, Tyr236 might be involved in a σ -bond tunneling through the “Trp191–Asp235–Tyr236” pathway; Tyr203 and the nearby Tyr251 might instead be implicated in a kind of T-shaped π stacking interaction that favors the ET along a pathway that comprises Trp191 and Phe202 residues.

ASSOCIATED CONTENT

Supporting Information

QM/MM scheme; more computational details and tables; additional EPR and UV-vis results. This material is available free of charge via the Internet at <http://pubs.acs.org>.

AUTHOR INFORMATION

Corresponding Author

*E-mail: adalgisa.sinicropi@unisi.it.

Notes

The authors declare no competing financial interest.

ACKNOWLEDGMENTS

We acknowledge the CINECA Awards N. HP10CJ65S2 and HP10CXBWGO and C.R.E.A (Centro Ricerche Energia e Ambiente, Colle Val D’Elsa, Siena, Italy) for the availability of high performance computing resources and support. This work was supported by the Italian MIUR PRIN09 project no. 2009STNWX3_001.

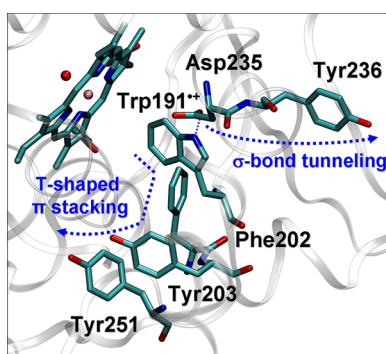


Figure 8. Possible electron transfer pathways involving Trp191^{•+}, Tyr203[•], and Tyr251[•].

■ REFERENCES

- (1) Altschul, A. M.; Abrams, R.; Hogness, T. R. Cytochrome C Peroxidase. *J. Biol. Chem.* **1940**, *136*, 777–794.
- (2) Jordi, H. C.; Erman, J. E. Cytochrome c Peroxidase Catalyzed Oxidation of Ferrocyanide by Hydrogen Peroxide. Transient State Kinetics. *Biochemistry* **1974**, *13*, 3734–3741.
- (3) Poulos, T. L. Thirty Years of Heme Peroxidase Structural Biology. *Arch. Biochem. Biophys.* **2010**, *500*, 3–12.
- (4) Yonetani, T.; Schleyer, H.; Ehrenberg, A. Studies on Cytochrome c Peroxidase: VII. Electron Paramagnetic Resonance Absorptions of the Enzyme and Complexes in Dissolved and Crystalline Forms. *J. Biol. Chem.* **1966**, *241*, 3240–3243.
- (5) Hoffman, B. M.; Roberts, J. E.; Kang, C. H.; Margoliash, E. Electron Paramagnetic and Electron Nuclear Double Resonance of the Hydrogen Peroxide Compound of Cytochrome c Peroxidase. *J. Biol. Chem.* **1981**, *256*, 6556–6564.
- (6) Sivaraja, M.; Goodin, D. B.; Smith, M.; Hoffman, B. M. Identification by ENDOR of Trp191 as the Free-Radical Site in Cytochrome c Peroxidase Compound ES. *Science* **1989**, *245*, 738–740.
- (7) Fishel, L. A.; Farnum, M. F.; Mauro, J. M.; Miller, M. A.; Kraut, J. Compound I Radical in Site-Directed Mutants of Cytochrome c Peroxidase as Probed by Electron Paramagnetic Resonance and Electron-Nuclear Double Resonance. *Biochemistry* **1991**, *30*, 1986–1996.
- (8) Huyett, J. E.; Doan, P. E.; Gurbiel, R.; Houseman, A. L. P.; Sivaraja, M.; Goodin, D. B.; Hoffman, B. M. Compound ES of Cytochrome c Peroxidase Contains a Trp π -Cation Radical: Characterization by CW and Pulsed Q-Band ENDOR Spectroscopy. *J. Am. Chem. Soc.* **1995**, *117*, 9033–9041.
- (9) Houseman, A. L. P.; Doan, P. E.; Goodin, D. B.; Hoffman, B. M. Comprehensive Explanation of the Anomalous EPR Spectra of Wild-Type and Mutant Cytochrome c Peroxidase Compound ES. *Biochemistry* **1993**, *32*, 4430–4443.
- (10) Fishel, L. A.; Villafranca, J. E.; Mauro, J. M.; Kraut, J. Yeast Cytochrome c Peroxidase: Mutagenesis and Expression in Escherichia coli show Tryptophan-51 is not the Radical Site in Compound I. *Biochemistry* **1987**, *26*, 351–360.
- (11) Mauro, J. M.; Fishel, L. A.; Hazzard, J. T.; Meyer, T. E.; Tollin, G.; Cusanovich, M. A.; Kraut, J. Tryptophan-191 \rightarrow Phenylalanine, a Proximal-Side Mutation in Yeast Cytochrome c Peroxidase that Strongly Affects the Kinetics of Ferrocytocochrome c Oxidation. *Biochemistry* **1988**, *27*, 6243–6256.
- (12) Ivancich, A.; Dorlet, P.; Goodin, D. B.; Un, S. Multifrequency High-Field EPR Study of the Tryptophanyl and Tyrosyl Radical Intermediates in Wild-Type and the W191G Mutant of Cytochrome c Peroxidase. *J. Am. Chem. Soc.* **2001**, *123*, 5050–5058.
- (13) Faller, P.; Goussias, C.; Rutherford, A. W.; Un, S. Resolving Intermediates in Biological Proton-Coupled Electron Transfer: A Tyrosyl Radical Prior to Proton Movement. *Proc. Natl. Acad. Sci. U.S.A.* **2003**, *100*, 8732–8735.
- (14) Himo, F.; Eriksson, L. A. Theoretical Study of Model Tryptophan Radicals and Radical Cations: Comparison with Experimental Data of DNA Photolyase, Cytochrome c Peroxidase, and Ribonucleotide Reductase. *J. Phys. Chem. B* **1997**, *101*, 9811–9819.
- (15) Menyhárd, D. K.; Náray-Szabó. Electrostatic Effect on Electron Transfer at the Active Site of Heme Peroxidases: A Comparative Molecular Orbital Study on Cytochrome C Peroxidase and Ascorbate Peroxidase. *J. Phys. Chem. B* **1999**, *103*, 227–233.
- (16) Krauss, M.; Garmer, D. Assignment of the Spectra of Protein Radicals in Cytochrome c Peroxidase. *J. Phys. Chem.* **1993**, *97*, 831.
- (17) Wirstam, M.; Blomberg, M. R. A.; Siegbahn, P. E. M. Reaction Mechanism of Compound I Formation in Heme Peroxidases: A Density Functional Theory Study. *J. Am. Chem. Soc.* **1999**, *121*, 10178–10185.
- (18) Bernini, C.; Pogni, R.; Ruiz-Dueñas, F. J.; Martínez, A. T.; Basosi, R.; Sinicropi, A. EPR Parameters of Amino Acid Radicals in *P. eryngii* Versatile Peroxidase and its W164Y variant computed at the QM/MM level. *Phys. Chem. Chem. Phys.* **2011**, *13*, 5078–5098.
- (19) Bernini, C.; Pogni, R.; Basosi, R.; Sinicropi, A. Prediction of Hydrogen-Bonding Networks around Tyrosyl Radical in *P. eryngii* Versatile Peroxidase W164Y Variants: a QM/MM MD Study. *Mol. Simul.* **2014**, *40*, 485–490.
- (20) Bernini, C.; Andruniów, T.; Olivucci, M.; Pogni, R.; Basosi, R.; Sinicropi, A. Effects of the Protein Environment on the Spectral Properties of Tryptophan Radicals in *Pseudomonas aeruginosa* Azurin. *J. Am. Chem. Soc.* **2013**, *135*, 4822–4833.
- (21) Bonagura, C. A.; Bhaskar, B.; Shimizu, H.; Sundaramoorthy, M.; McRee, D. E.; Goodin, D. B.; Poulos, T. L. High-Resolution Crystal Structures and Spectroscopy of Native and Compound I Cytochrome c Peroxidase. *Biochemistry* **2003**, *42*, 5600–5608.
- (22) Li, H.; Robertson, A. D.; Jensen, J. H. Very Fast Empirical Prediction and Rationalization of Protein pK_a Values. *Proteins: Struct., Funct., Bioinf.* **2005**, *61*, 704–721.
- (23) Humphrey, W.; Dalke, A.; Schulter, K. VMD - Visual Molecular Dynamics. *J. Mol. Graphics* **1996**, *14*, 33–38.
- (24) Jorgensen, W. L.; Chandrasekhar, J.; Madura, J. D.; Impey, R. W.; Klein, M. L. Comparison of Simple Potential Functions for Simulating Liquid Water. *J. Chem. Phys.* **1983**, *79*, 926–935.
- (25) Cornell, W. D.; Cieplak, P.; Bayly, C. I.; Gould, I. R.; Merz, K. M.; Ferguson, D. M.; Spellmeyer, D. C. A Second Generation Force Field for the Simulation of Proteins, Nucleic Acids, and Organic Molecules. *J. Am. Chem. Soc.* **1995**, *117*, 5179–5197.
- (26) Wang, J.; Cieplak, P.; Kollman, P. A. How Well Does a Restrained Electrostatic Potential (RESP) Model Perform in Calculating Conformational Energies of Organic and Biological Molecules? *J. Comput. Chem.* **2000**, *21*, 1049–1074.
- (27) Ponder, J. W.; Case, D. A. Force Fields for Protein Simulations. *Adv. Protein Chem.* **2003**, *66*, 27–85.
- (28) <http://www.pharmacy.manchester.ac.uk/bryce/amber/>.
- (29) Frisch, M. J.; Trucks, G. W.; Schlegel, H. B.; Scuseria, G. E.; Robb, M. A.; Cheeseman, J. R.; Montgomery, J. A., Jr.; Vreven, T.; Kudin, K. N.; Burant, J. C.; Millam, J. M.; Iyengar, S. S.; Tomasi, J.; Barone, V.; Mennucci, B.; Cossi, M.; Scalmani, G.; Rega, N.; Petersson, G. A.; Nakatsuji, H.; Hada, M.; Ehara, M.; Toyota, K.; Fukuda, R.; Hasegawa, J.; Ishida, M.; Nakajima, T.; Honda, Y.; Kitao, O.; Nakai, H.; Klene, M.; Li, X.; Knox, J. E.; Hratchian, H. P.; Cross, J. B.; Bakken, V.; Adamo, C.; Jaramillo, J.; Gomperts, R.; Stratmann, R. E.; Yazyev, O.; Austin, A. J.; Cammi, R.; Pomelli, C.; Ochterski, J.; Ayala, P. Y.; Morokuma, K.; Voth, G. A.; Salvador, P.; Dannenberg, J. J.; Zakrzewski, V. G.; Dapprich, S.; Daniels, A. D.; Strain, M. C.; Farkas, O.; Malick, D. K.; Rabuck, A. D.; Raghavachari, K.; Foresman, J. B.; Ortiz, J. V.; Cui, Q.; Baboul, A. G.; Clifford, S.; Cioslowski, J.; Stefanov, B. B.; Liu, G.; Liashenko, A.; Piskorz, P.; Komaromi, I.; Martin, R. L.; Fox, D. J.; Keith, T.; Al-Laham, M. A.; Peng, C. Y.; Nanayakkara, A.; Challacombe, M.; Gill, P. M. W.; Johnson, B. G.; Chen, W.; Wong, M. W.; Gonzalez, C.; Pople, J. A. *Gaussian* 03, Revision B.04; Gaussian, Inc.: Wallingford, CT, 2004.
- (30) Phillips, J. C.; Braun, R.; Wang, W.; Gumbart, J.; Tajkhorshid, E.; Villa, E.; Chipot, C.; Skeel, R. D.; Kale, L.; S. K. Scalable Molecular Dynamics with NAMD. *J. Comput. Chem.* **2005**, *26*, 1781–1802.
- (31) Darden, T.; York, D.; Pederson, L. Particle Mesh Ewald: An N-log(N) Method for Ewald Sums in Large Systems. *J. Chem. Phys.* **1993**, *98*, 10089–10092.
- (32) Aquilante, F.; De Vico, L.; Ferré, N.; Ghigo, G.; Malmqvist, P.-Å.; Neogrády, P.; Pedersen, T. B.; Pitonak, M.; Reiher, M.; Roos, B. O.; Serrano-Andrés, L.; Urban, M.; Veryazov, V.; Lindh, R. MOLCAS 7: The Next Generation. *J. Comput. Chem.* **2010**, *31*, 224–247.
- (33) Ponder, J. W. *Tinker* 4.2, software tools for molecular design; 2004; <http://dasher.wustl.edu/tinker>.
- (34) Ferré, N.; Olivucci, M. The Amide Bond: Pitfalls and Drawbacks of the Link Atom Scheme. *J. Mol. Struct.: THEOCHEM* **2003**, *632*, 71–82.
- (35) Ferré, N.; Olivucci, M. Probing the Rhodopsin Cavity with Reduced Retinal Models at the CASPT2//CASSCF/AMBER Level of Theory. *J. Am. Chem. Soc.* **2003**, *125*, 6868–6869.
- (36) Andruniów, T.; Ferré, N.; Olivucci, M. Structure, Initial Excited-State Relaxation, and Energy Storage of Rhodopsin Resolved at the

- Multiconfigurational Perturbation Theory Level. *Proc. Natl. Acad. Sci. U.S.A.* **2004**, *101*, 17908–17913.
- (37) Pistolesi, S.; Sinicropi, A.; Pogni, R.; Basosi, R.; Ferré, N.; Olivucci, M. Modeling the Fluorescence of Protein-Embedded Tryptophans with ab Initio Multiconfigurational Quantum Chemistry: The Limiting Cases of Parvalbumin and Monellin. *J. Phys. Chem. B* **2009**, *113*, 16082–16090.
- (38) Sinicropi, A.; Andruriow, T.; Ferré, N.; Basosi, R.; Olivucci, M. Properties of the Emitting State of the Green Fluorescent Protein resolved at the CASPT2//CASSCF/CHARMM Level. *J. Am. Chem. Soc.* **2005**, *127*, 11534–11535.
- (39) Frisch, M. J.; Trucks, G. W.; Schlegel, H. B.; Scuseria, G. E.; Robb, M. A.; Cheeseman, J. R.; Scalmani, G.; Barone, V.; Mennucci, B.; Petersson, G. A.; Nakatsuji, H.; Caricato, M.; Li, X.; Hratchian, H. P.; Izmaylov, A. F.; Bloino, J.; Zheng, G.; Sonnenberg, J. L.; Hada, M.; Ehara, M.; Toyota, K.; Fukuda, R.; Hasegawa, J.; Ishida, M.; Nakajima, T.; Honda, Y.; Kitao, O.; Nakai, H.; Vreven, T.; Montgomery, J. A.; Peralta, J. E.; Ogliaro, F.; Bearpark, M.; Heyd, J. J.; Brothers, E.; Kudin, K. N.; Staroverov, V. N.; Keith, T.; Kobayashi, R.; Normand, J.; Raghavachari, K.; Rendell, A.; Burant, J. C.; Iyengar, S. S.; Tomasi, J.; Cossi, M.; Rega, N.; Millam, J. M.; Klene, M.; Knox, J. E.; Cross, J. B.; Bakken, V.; Adamo, C.; Jaramillo, J.; Gomperts, R.; Stratmann, R. E.; Yazayev, O.; Austin, A. J.; Cammi, R.; Pomelli, C.; Ochterski, J. W.; Martin, R. L.; Morokuma, K.; Zakrzewski, V. G.; Voth, G. A.; Salvador, P.; Dannenberg, J. J.; Dapprich, S.; Daniels, A. D.; Farkas, O.; Foresman, J. B.; Ortiz, J. V.; Cioslowski, J.; Fox, D. J. *Gaussian* 09, Revision B.01; Gaussian, Inc.: Wallingford, CT, 2010.
- (40) Zhang, H.; He, S.; Mauk, A. G. Radical Formation at Tyr39 and Tyr153 Following Reaction of Yeast Cytochrome c Peroxidase with Hydrogen Peroxide. *Biochemistry* **2002**, *36*, 13507–13513.
- (41) Musah, R. A.; Goodin, D. B. Introduction of Novel Substrate Oxidation into Cytochrome c Peroxidase by Cavity Complementation: Oxidation of 2-Aminothiazole and Covalent Modification of the Enzyme. *Biochemistry* **1997**, *36*, 11665–11674.
- (42) Barrows, T. P.; Bhaskar, B.; Thomas, L. P. Electrostatic Control of the Tryptophan Radical in Cytochrome c Peroxidase. *Biochemistry* **2004**, *43*, 8826–8834.
- (43) Neese, F. ORCA, version 2.9, an ab initio, density functional and semiempirical program package; Max Planck-Institute for Bioinorganic Chemistry: Mülheim a.d. Ruhr, Germany, 2012.
- (44) Becke, A. D. Density Functional Thermochemistry. III. The Role of Exact Exchange. *J. Chem. Phys.* **1993**, *98*, 5648–5652.
- (45) Lee, C.; Yang, W.; Parr, R. G. Development of the Colle-Salvetti Correlation-Energy Formula into a Functional of the Electron Density. *Phys. Rev. B* **1988**, *37*, 785–789.
- (46) Stephens, P. J.; Devlin, F. J.; Chabalowski, C. F.; Frisch, M. J. Ab Initio Calculation of Vibrational Absorption and Circular Dichroism Spectra Using Density Functional Force Fields. *J. Phys. Chem.* **1994**, *98*, 11623–11627.
- (47) Barone, V. *Recent Advances in Density Functional Methods, Part I*; Chong, D. P. Ed.; World Scientific Publishing Co.: River Edge, NJ, 1995.
- (48) Barone, V.; Polimeno, A. Toward an Integrated Computational Approach to CW-ESR Spectra of Free Radicals. *Phys. Chem. Chem. Phys.* **2006**, *8*, 4609–4629.
- (49) Godbout, N.; Salahub, D. R.; Andzelm, J.; Wimmer, E. Optimization of Gaussian-Type Basis Sets for Local Spin Density Functional Calculations. Part I. Boron through Neon, Optimization Technique and Validation. *Can. J. Chem.* **1992**, *70*, 560–571.
- (50) Neese, F. Spin-Hamiltonian Parameters from First Principle Calculations: Theory and Application. In *High Resolution EPR*; Berliner, L., Hanson, G., Eds.; Springer: New York, 2009; Vol. 28, pp 175–229.
- (51) Bernini, C.; Sinicropi, A.; Basosi, R.; Pogni, R. Tyrosyl Radical in the W164Y Mutant of *P. eryngii* Versatile Peroxidase: an EPR and DFT/PCM Study. *Appl. Magn. Reson.* **2010**, *37*, 279–288.
- (52) Svistunenko, D. A.; Jones, G. A. Tyrosyl Radicals in Proteins: A Comparison of Empirical and Density Functional Calculated EPR Parameters. *Phys. Chem. Chem. Phys.* **2009**, *11*, 6600–6613.
- (53) Schäfer, A.; Huber, C.; Ahlrichs, R. Fully Optimized Contracted Gaussian Basis Sets of Triple Zeta Valence Quality for Atoms Li to Kr. *J. Chem. Phys.* **1994**, 5829–5835.
- (54) Sinnecker, S.; Slep, L. D.; Bill, E.; Neese, F. Performance of Nonrelativistic and Quasi-Relativistic Hybrid DFT for the Prediction of Electric and Magnetic Hyperfine Parameters in ^{57}Fe Mössbauer Spectra. *Inorg. Chem.* **2005**, *44*, 2245–2254.
- (55) Neese, F. Efficient and Accurate Approximations to the Molecular Spin-Orbit Coupling Operator and Their Use in Molecular g-Tensor Calculations. *J. Chem. Phys.* **2005**, *122*, 034107–034113.
- (56) Kampa, M.; Pandelia, M.-E.; Lubitz, W.; van Gastel, M.; Neese, F. A Metal–Metal Bond in the Light-Induced State of $[\text{NiFe}]$ Hydrogenases with Relevance to Hydrogen Evolution. *J. Am. Chem. Soc.* **2013**, *135*, 3915–3925.
- (57) Patanzis, D. A.; Chen, X.-Y.; Landis, C. R.; Neese, F. All-Electron Scalar Relativistic Basis Sets for Third-Row Transition Metal Atoms. *J. Chem. Theory Comput.* **2008**, *4*, 908–919.
- (58) Radoul, M.; Sundararajan, M.; Potapov, A.; Ripplinger, C.; Neese, F.; Goldfarb, D. Revisiting the Nitrosyl Complex of Myoglobin by High-Field Pulse EPR Spectroscopy and Quantum Mechanical Calculations. *Phys. Chem. Chem. Phys.* **2010**, *12*, 7276–7289.
- (59) Weigend, F.; Ahlrichs, R. Balanced Basis Sets of Split Valence, Triple Zeta Valence and Quadruple Zeta Valence Quality for H to Rn: Design and Assessment of Accuracy. *Phys. Chem. Chem. Phys.* **2005**, *7*, 3297–3305.
- (60) Eichkorn, K.; Weigend, F.; Treutler, O.; Ahlrichs, R. Auxiliary Basis Sets for Main Row Atoms and Transition Metals and Their Use to Approximate Coulomb Potentials. *Theor. Chem. Acc.* **1997**, *97*, 119–124.
- (61) Neese, F. Prediction and Interpretation of the ^{57}Fe Isomer Shift in Mössbauer Spectra by Density Functional Theory. *Inorg. Chim. Acta* **2002**, *337*, 181–192.
- (62) Schäfer, A.; Horn, H.; Ahlrichs, R. Fully Optimized Contracted Gaussian Basis Sets for Atoms Li to Kr. *J. Chem. Phys.* **1992**, *97*, 2571–2577.
- (63) Petrenko, T.; Neese, F. Analysis and Prediction of Absorption Band Shapes, Fluorescence Band Shapes, Resonance Raman Intensities, and Excitation Profiles using the Time-Dependent Theory of Electronic Spectroscopy. *J. Chem. Phys.* **2007**, *127*, 164319.
- (64) Bleifuss, G.; Kolberg, M.; Pötsch, S.; Hofbauer, W.; Bittl, R.; Lubitz, W.; Gräslund, A.; Lassmann, G.; Lendzian, F. Tryptophan and Tyrosine Radicals in Ribonucleotide Reductase: A Comparative High-Field EPR Study at 94 GHz. *Biochemistry* **2001**, *40*, 15362–15368.
- (65) Bernini, C.; Pogni, R.; Basosi, R.; Sinicropi, A. The Nature of Tryptophan Radicals Involved in the Long-Range Electron Transfer of Lignin Peroxidase and Lignin Peroxidase-like Systems: Insights from Quantum Mechanical/Molecular Mechanics Simulations. *Proteins: Struct., Funct., Bioinf.* **2012**, *80*, 1476–1483.
- (66) Svistunenko, D. A.; Adelusi, M.; Dawson, M.; Robinson, P.; Bernini, C.; Sinicropi, A.; Basosi, R. Computation Informed Selection of Parameters for Protein Radical EPR Spectra Simulation. *Stud. Univ. Babes-Bolyai, Chem.* **2011**, *56*, 135–146.
- (67) Un, S. The G-Values and Hyperfine Coupling of Amino Acid Radicals in Proteins: Comparison of Experimental Measurements with Ab Initio Calculations. *Magn. Reson. Chem.* **2005**, *43*, S229–S236.
- (68) Stoll, S.; Shafaat, H. S.; Krzystek, J.; Ozarowski, A.; Tauber, M. J.; Kim, J. E.; Britt, R. D. Hydrogen Bonding of Tryptophan Radicals Revealed by EPR at 700 GHz. *J. Am. Chem. Soc.* **2011**, *133*, 18098–18101.
- (69) Solar, S.; Getoff, N.; Surdhar, P. S.; Armstrong, D. A.; Singh, A. Oxidation of Tryptophan and N-Methylindole by N_3^{\bullet} , $\text{Br}_2^{\bullet-}$, and $(\text{SCN})_2^{\bullet-}$ Radicals in Light- and Heavy-Water Solutions: A Pulse Radiolysis Study. *J. Phys. Chem.* **1991**, *95*, 3639–3643.
- (70) Bellina, B.; Compagnon, I.; Houver, S.; Maitre, P.; Allouche, A.-R.; Antoine, R.; Dugourd, P. Spectroscopic Signatures of Peptides Containing Tryptophan Radical Cations. *Angew. Chem., Int. Ed.* **2011**, *50*, 11430–11432.

- (71) Joly, L.; Antoine, R.; Allouche, A.-R.; Dugourd, P. Formation and Spectroscopy of a Tryptophan Radical Containing Peptide in the Gas Phase. *J. Am. Chem. Soc.* **2008**, *130*, 13832–13833.
- (72) Shafaat, H. S.; Leigh, B. S.; Tauber, M. J.; Kim, J. E. Spectroscopic Comparison of Photogenerated Tryptophan Radicals in Azurin: Effects of Local Environment and Structure. *J. Am. Chem. Soc.* **2010**, *132*, 9030–9039.
- (73) Yonetani, T.; Ray, G. S. Studies on Cytochrome c Peroxidase. I. Purification and Some Properties. *J. Biol. Chem.* **1965**, *240*, 4503–4508.
- (74) Schünemann, V.; Lendzian, F.; Jung, C.; Contzen, J.; Barra, A. L.; Sligar, S. G.; Trautwein, A. X. Enzyme Catalysis and Regulation: Tyrosine Radical Formation in the Reaction of Wild Type and Mutant Cytochrome P450cam with Peroxy Acids: A Multifrequency EPR Study of Intermediates on the Millisecond Time Scale. *J. Biol. Chem.* **2004**, *279*, 10919–10930.
- (75) Carrington, A.; McLachlan, A. D. *Introduction to Magnetic Resonance*; Harper & Row: New York, 1969.
- (76) Un, S.; Gerez, C.; Elleingand, E.; Fontecave, M. Sensitivity of Tyrosyl Radical g-Values to Changes in Protein Structure: A High-Field EPR Study of Mutants of Ribonucleotide Reductase. *J. Am. Chem. Soc.* **2001**, *123*, 3048–3054.
- (77) Ivancich, A.; Mazza, G.; Desbois, A. Comparative Electron Paramagnetic Resonance Study of Radical Intermediates in Turnip Peroxidase Isozymes. *Biochemistry* **2001**, *40*, 6860–6866.
- (78) Ivancich, A.; Mattioli, T. A.; Un, S. Effect of Protein Microenvironment on Tyrosyl Radicals. A High-Field (285 GHz) EPR, Resonance Raman, and Hybrid Density Functional Study. *J. Am. Chem. Soc.* **1999**, *121*, 5743–5753.
- (79) Hart, R.; O’Malley, P. J. A Quantum Mechanics/Molecular Mechanics Study of the Tyrosine Residue, Tyr_D, of Photosystem II. *Biochim. Biophys. Acta* **2010**, *1797*, 250–254.
- (80) Matsuoka, H.; Shen, J.-R.; Kawamori, A.; Nishiyama, K.; Ohba, Y.; Yamauchi, S. Proton-Coupled Electron-Transfer Processes in Photosystem II Probed by Highly Resolved g-Anisotropy of Redox-Active Tyrosine Y_Z. *J. Am. Chem. Soc.* **2011**, *133*, 4655–4660.
- (81) Kim, S. H.; Aznar, C.; Brynda, M.; Silks, L. A.; Michalczyk, R.; Unkefer, C. J.; Woodruff, W. H.; Britt, R. D. An EPR, ESEEM, Structural NMR, and DFT Study of a Synthetic Model for the Covalently Ring-Linked Tyrosine-Histidine Structure in the Heme-Copper Oxidases. *J. Am. Chem. Soc.* **2004**, *126*, 2328–2338.
- (82) Un, S.; Tang, X.-S.; Diner, B. A. 245 GHz High-Field EPR Study of Tyrosine-D° and Tyrosine-Z° in Mutants of Photosystem II. *Biochemistry* **1996**, *35*, 679–684.